# Quantum-classical modeling of photoisomerization of polyatomic molecules

D. C. Tranca and A. A. Neufeld

Citation: The Journal of Chemical Physics **132**, 134109 (2010); doi: 10.1063/1.3368644
View online: http://dx.doi.org/10.1063/1.3368644
View Table of Contents: http://scitation.aip.org/content/aip/journal/jcp/132/13?ver=pdfcov
Published by the AIP Publishing

# Quantum-classical modeling of photoisomerization of polyatomic molecules

D. C. Tranca and A. A. Neufeld[a)]
*Abteilung Spektroskopie und Photochemische Kinetik, Max-Planck-Institut für Biophysikalische Chemie, Am Fassberg, D-37077 Göttingen, Germany*

(Received 15 December 2009; accepted 2 March 2010; published online 6 April 2010)

A new method, non-Markovian quantum-classical approximation (NQCA), is suggested to model the photoisomerization of polyatomic molecules. The NQCA method can be successfully applied to follow the photoisomerization process for a wide class of reacting systems, namely, those for which the time scale required for the equilibration in the phase space of the potential energy surface (PESs) is short compared to the time scale of the transitions between them. Such a situation is quite typical for the nonadiabatic transitions between the different electronic states in polyatomic molecules, where a high density of vibronic states facilitates the intramolecular vibrational energy redistribution, thus providing an efficient relaxation for the phase space distribution. The NQCA can easily be combined with molecular dynamics and quantum-chemical methods to describe the evolution of the classical degrees of freedom and the quantum part of the problem. © *2010 American Institute of Physics*. [doi:10.1063/1.3368644]

## I. INTRODUCTION

Nonadiabatic processes play an important role in a variety of chemical and biological reactions, such as electron/proton/energy transfer,[1–3] isomerization, etc. The breakdown of the adiabatic Born–Oppenheimer approximation usually takes place when the energy splitting between the adiabatic potential energy surfaces, obtained at the fixed positions of the atomic nuclei, becomes comparable to the nonadiabatic coupling terms, so that it can no longer be taken into consideration by means of pertubation theory. These regions of the nonadiabaticity are typically characterized by a high efficiency of the transitions between the quantum states involved.

The nonadiabatic dynamics of small systems (i.e., with a few degrees of freedom) is well investigated by now using both fully quantum-mechanical treatments[4] and approximate approaches ranging from the rigorous semiclassical[4–7] ones to the various hybrid schemes adding quantum transitions to classical trajectories, e.g., surface hopping[5,6] and mean-field approximation.[5,6]

However, most of the realistic reaction complexes involve polyatomic molecules for which the reaction coordinates are often multidimensional, fact which restricts the range of applicable methods to the quantum-classical approaches.[5,6,8,9] The quantum-classical methods use classical mechanics to describe the dynamics of nuclei on the given PES, while keeping a quantum-mechanical treatment for the transitions between them. These methods also exhibit a linear scaling with the increase of the number of the degrees of freedom which making them applicable to the study of the nonadiabatic dynamics of polyatomic reacting systems.

A key problem in any *ab initio* approach to the quantum transitions is the accurate and consistent treatment of the transition phase. In the case of the nonadiabatic dynamics, when the transitions often lead to a considerable reorganization of the reaction complexes, the *ab initio* approach has to account both for the detailed balance and for the quantum coherence effects. A non-Markovian quantum-classical approximation (NQCA) (Ref. 8) has several advantages over other hybrid quantum-classical approaches in use.[5–7] Thus, it has known and wide applicability limits and is capable of the dynamic treatment of the transitions with a full account of the free-energy change in the course of the transitions, quantum interference, and memory effects. The method can also be easily applied to realistic multidimensional reaction coordinates through the use of an *ab initio* molecular dynamics technique.

In the present article the NQCA method has been used to study the nonadiabatic pathway for the photoisomerization reaction of *trans*-stilbene and p-coumaric acid molecules, both these molecules are subject of intensive theoretical[10] and experimental investigations.[11–13] The first one (*trans*-stilbene) has a large fluorescence quantum yield and an ability to follow the isomerization reaction in a variety of environments from the single molecule to solvents and molecular clusters. The second molecule (p-coumaric acid) is the cromophore responsible for the light absorption in photoactive yellow protein which functions as the blue light sensor in certain bacteria. However, despite an apparent similarity of these two molecules and of the underlying photoisomerization mechanism, the p-coumaric acid has an isomerization rate about hundred times faster than that of the *trans*-stilbene.

The outline of this paper is as follows. In Sec. II the basic definitions and assumptions regarding the simulation procedures of the photoisomerization processes are introduced. The corresponding kinetic equations of the

[a)]Electronic mail: aneufel@gwdg.de.

 

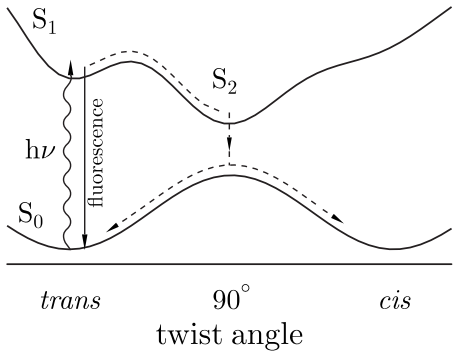


FIG. 1. Schematic representation of the adiabatic model for the *trans-cis* photoisomerization of stilbene and stilbenelike molecules. It assumes the existence of a small barrier in the first excited state PES and fast IVR. Activated barrier crossing is assumed to be the rate limiting step, a radiationless transition into the ground state takes place from the twisted conformation, which nevertheless belongs to the distinct electron PES.

quantum-classical approach used for the simulations of the photoisomerization of polyatomic molecules are described in Sec. III. The results obtained are presented and discussed in Sec. IV. In Sec. V we summarize the results obtained.

## II. BASIC ASSUMPTIONS

Two models were suggested in the literature to explain the mechanism of the photoinduced isomerization of *trans*-stilbene and similar systems and to simulate the corresponding experimental data.[14–19] In an adiabatic model,[14,15] see Fig. 1, one assumes the existence of a small barrier on the first excited state ($S_1$) and fast intramolecular vibrational energy redistribution (IVR), so that the Rice–Ramsperger–Kassel–Marcus (RRKM) model can be used to calculate the reaction rate.[20,21] The adiabatic model was successfully applied to the description of the molecular beam experiments[18,22] and an effective barrier height was estimated to be about 1200 $cm^{-1}$. However, the pressure dependence of the reaction rate is not well reproduced and its description requires the introduction/assumption of a "pressure dependent barrier," without any physically clear picture. In particular, at low pressures the theoretical model fits reasonably well to the experimental data,[23,24] but at pressures above 5 bar the experimental rate constant levels off at 20–30 $ns^{-1}$, while the theoretical high-pressure limit[24] is at 76 $ns^{-1}$. Alternatively, a nonadiabatic model involving the transition to another excited state was suggested[16–19] in order to explain the photoisomerization mechanism. This model is supported by the fact that the twisted conformation of stilbene, where the radiationless transition to the ground state takes place, belongs to the distinct electronic state ($S_2$) characterized as the doubly excited or zwitterionic state.[16–19]

The origin of the small barrier in the adiabatic model for the twist around the central ethylenic bond, which is also assumed to be the reaction coordinate, is not clear. A bond length is typically a good qualitative measure for the electron density located on it and for the associated barrier height of the torsional motion around it. The longer the bond length, the lower the barrier, and vice-versa. A series of accurate quantum-chemical calculations (done by us with the GAMESS U.S. software at the MCSCF level) show (see Table I) that in the ground state the central ethylenic bond ($C_7$—$C_8$ in Fig. 2) of *trans*-stilbene has a double bond character with the length of about 1.36 Å [this is in good agreement with previous reported values for this bond, of 1.354/1.33 Å (Refs. 25–28)], whereas the neighboring ones ($C_2$—$C_7$, $C_8$—$C_9$) have more a single bond character with the length of about 1.47 Å (1.483/1.45 Å according to Refs. 25–28). As a result, the direct twist around the central bond in the ground state has a large activation barrier, while the potential energy surface for the twist of the phenyl rings is flat in the range of about 30°.[29,30] The results of the bond lengths for *trans*-stilbene molecule are also summarized in the Table I.

TABLE I. In this table are given the bond lengths for the central ethylenic bond ($C_7$—$C_8$) and for the neighboring ones ($C_2$—$C_7$, $C_8$—$C_9$) for *trans*-stilbene.

| *Trans*-stilbene electronic structure calculations | Bond lengths | | |
|---|---|---|---|
| | $C_2$—$C_7$ | $C_7$—$C_8$ | $C_8$—$C_9$ |
| Ground state ($S_0$) | 1.47 | 1.36 | 1.47 |
| First excited state ($S_1$) | 1.41 | 1.40 | 1.41 |
| Second excited state ($S_2$) | 1.39 | 1.44 | 1.39 |

On the other hand, in the first exited state the corresponding lengths are estimated to be 1.40 Å (1.432 Å according to Refs. 25–28) for the central ethylenic bond ($C_7$—$C_8$ shown in Table I) and 1.41 Å (1.419 Å according to Refs. 25–28) for the neighboring ones ($C_2$—$C_7$, $C_8$—$C_9$), which is in between the single (~1.5 Å) and the double bond character (~1.35 Å). As a result, the twist around the central bond is still expected to have a considerable barrier. In this state the molecule still maintain the planar configuration.[25,31]

Finally, our quantum-chemical calculations have shown that in the doubly excited state the central bond has the length of 1.45 Å, shown in Table I, which is closer to the single bond character. Thus, in the double excited state the twist around the central ethylenic bond could be almost barrierless.

Thus, the nonadiabatic pathway of the photoisomerization, involving the preliminary transition from $S_1$ to $S_2$ state within the planar geometry of *trans*-stilbene, should be favored over the direct twist around the central bond in the $S_1$ state. In this case the twist around the central bond is not considered as the rate limiting step, and the reaction coordi-

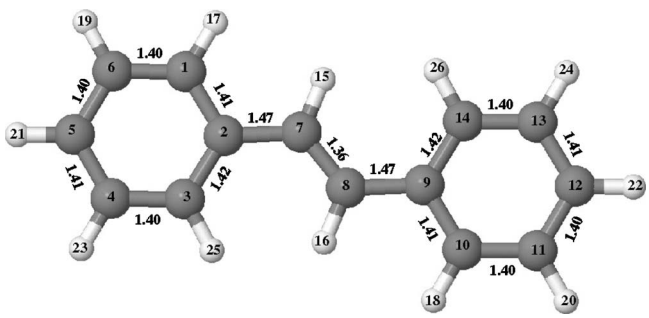


FIG. 2. Schematic representation of *trans*-stilbene and its bond lengths for the ground ($S_0$) state. Carbon atoms are represented through gray balls, whereas the hydrogen atoms through white balls.

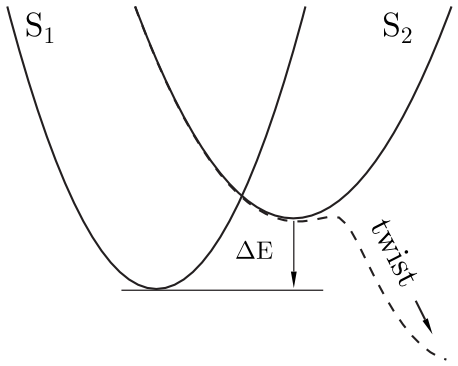


FIG. 3. Schematic model for the *trans-cis* nonadiabatic photoisomerization process. The PESs have been considered to be diabatic. It assumes fast IVR and the nonadiabatic conversion from the first excited state ($S_1$) into the double excited one ($S_2$) near the planar geometry to be the rate limiting step. The subsequent twist around the central bond proceeds along $S_2$ PES where it is considered to be nearly barrierless. The X-axis is taken to be the reaction coordinate.

nate for the $S_1 \rightarrow S_2$ conversion can be any, including in-plane vibrations. For example, it was found in Ref. 18 that the nonadiabatic RRKM fits well the experimental data if one uses a normal mode with the frequency of 400 $cm^{-1}$ as the reaction coordinate which is obviously not the frequency of the twist around the central bond.

We estimate the efficiency of the nonadiabatic pathway of the photoisomerization based on a model which consist of two multidimensional PESs as schematically shown in Fig. 3. We assume that the molecule in first excited state $S_1$ is prepared with a small energy excess (the frequency of the laser pulse is about the 0–0 transition frequency), so that the energy distribution on $S_1$ PES may be considered as the canonical one with the temperature $T$ of the surrounding media, possibly corrected to account for the vibrational cooling effect.

The PESs for the $S_1$ and $S_2$ states near their planar geometry were obtained in the normal modes approximation by using the quantum-chemical GAMESS U.S. software at the MCSCF level. This should be a reasonably good approximation for all modes except for the twist around the central ethylenic bond in $S_2$ state, which is nearly barrierless as it was mentioned above. The IVR in *trans*-stilbene is fast, compared to the time scale of the photoisomerization, and was estimated to take about 20 ps.[32–39] This makes the transition $S_1 \rightarrow S_2$ irreversible since the molecule very fast twists to the transition state with the energy, considerably lower than the minimum of the $S_1$ PES. Such a situation is similar to the nonadiabatic transitions in the "inverted region" of the free-energy-gap law where the transitions are thermally activated but irreversible. However, the normal modes approximation at the local energy minimum of $S_2$ PES near the planar geometry was used to restore the energy profile in the transition zone.

The energy splitting between the PESs plays a key role in the nonadiabatic dynamics. We estimated the energy gap between the minima of $S_2$ and $S_1$ states in *trans*-stilbene from the spectroscopical data and quantum-chemical calculations[40] (CASSCF/CASPT2 approach) to be about

TABLE II. In this table are given the bond lengths for the central ethylenic bond ($C_7$—$C_8$) and for the neighboring ones ($C_2$—$C_7$, $C_8$—$C_9$) for coumaric acid.

| Coumaric acid electronic structure calculations | Bond lengths | | |
|---|---|---|---|
| | $C_2$—$C_7$ | $C_7$—$C_8$ | $C_8$—$C_9$ |
| Ground state ($S_0$) | 1.48 | 1.35 | 1.48 |
| First excited state ($S_1$) | 1.39 | 1.39 | 1.47 |
| Second excited state ($S_2$) | 1.35 | 1.49 | 1.43 |

$\Delta E = E_2 - E_1 = 0.6$ eV (the minimum of $S_2$ PES lies above the minimum of $S_1$). More details about the calculations of the energy splitting between the PESs are given in Sec. III C. This value is rather large and seems to prevent any surface crossing events, since it requires too large (and rare) fluctuations of the energy per (reaction) degree of freedom. Nevertheless, in the canonical ensemble the $S_1 \rightarrow S_2$ transition is not forbidden energetically, although the mechanism of the nonadiabatic transitions in polyatomic molecules may fundamentally be different from those in small molecules. Within the classical mechanics picture, in the one-dimensional case the energetically allowed nonadiabatic transitions always proceed via the surface crossing events, whereas in the multidimensional case the fast IVR redistributes the energy among other degrees of freedom and may effectively prevent the surface crossing events.

Together with the *trans-cis* photoisomerization of stilbene, we consider the *trans-cis* photoisomerization of p-coumaric acid, schematically shown in Table II. The electronic structure calculations for the p-coumaric acid molecule have been done using the GAMESS U.S. software at the MCSCF level. Similarly to the *trans*-stilbene case we have found that the central bond ($C_7$—$C_8$), shown in Table II, in the ground state of p-coumaric acid has a double bond character (1.35 Å) which means that it has a large barrier preventing the rotation around it. The neighboring bonds ($C_2$—$C_7$, $C_8$—$C_9$) both have the length of about 1.48 Å which is close to the single bond character, thus making the corresponding potentials for the twist around them to be flat.

In the first excited state (see Table II) the length of the central bond and one of the neighboring bonds ($C_2$—$C_7$, $C_7$—$C_8$) becomes 1.39 Å, whereas the bond length $C_8$—$C_9$ is just slightly affected and becomes 1.47 Å. The rotation around the central bond will still have a to large energy barrier to allow for the photoisomerization process to take place in this state. Finally, in the doubly excited state (see Table II) the central bond has the length of 1.49 Å, which is of single bond character and the twist around it may again become nearly barriereless.

Thus, the quantum chemistry of p-coumaric acid and its photoisomerization mechanism look quite similar to the ones of *trans*-stilbene. However, the p-coumaric acid chromophore exhibits a much faster isomerization rate than that of *trans*-stilbene.[41–43] We attempt to clarify the origin of this difference below.

## III. NQCA AND THE PHOTOISOMERIZATION PROCESSES OF POLYATOMIC MOLECULES

### A. Basic equations of NQCA for the photoisomerization processes of polyatomic molecules

In the case of the two PESs the Hamiltonian of the system under consideration can be written as

$$\hat{H} = \hat{H}_N^{(1)}|1\rangle\langle 1| + \hat{H}_N^{(2)}|2\rangle\langle 2| + \hat{V}, \tag{1}$$

where $\hat{H}_N^{(1,2)}$ are the PESs Hamiltonians depending on the coordinates of the nuclei, $\hat{V}$ is the coupling Hamiltonian between them, and $|n\rangle\langle n|$ are the projectors on the $n$th electronic state. The coupling operator is determined as the scalar product of the momentum of the atomic central $\mathbf{p}_\alpha$ and the corresponding nonadiabatic coupling vector $\mathbf{d}_\alpha$

$$\hat{V} = -\sum_{\alpha=1}^{n} \frac{i\hbar}{m_\alpha} \mathbf{p}_\alpha \cdot \mathbf{d}_\alpha, \tag{2}$$

where the sum is taken over all atomic centers. In the above equation $\hbar$ is the Planck constant and $m_\alpha$ is the mass of the $\alpha$th atom in the molecule.

The kinetic equations of the quantum-classical approach, in the absence of the backward reaction, can be readily be obtained from those used in Ref. 44 by formally taking the limit of infinite negative free-energy change in the course of the reaction, and have the following form

$$\frac{d\sigma(t)}{dt} = -\lim_{N\to\infty} \frac{1}{N} \sum_{k=1}^{N} \mathrm{Im}(\chi_k(t) V_k(t)), \tag{3}$$

where $\sigma(t)$ is the probability of being on $S_1$ PES, $N$ is in practice a large number of classical trajectories sufficient to sample the phase space of $S_1$, and

$$\frac{d\chi_k(t)}{dt} = 2iV_k(t)\sigma(t) - i\Omega_k(t)\chi_k(t) \tag{4}$$

is the auxiliary function for the given trajectory, which accounts for the quantum phase and memory effects. The time dependence of the nonadiabatic coupling $V_k(t)$ and the PESs Hamiltonian functions difference $\Omega_k(t)$ (vertical energy gap) in Eqs. (3) and (4) is in accordance with the corresponding phase space trajectory $q_k(t)$, i.e.,

$$V_k(t) = -\sum_{\alpha=1}^{n} \frac{i\hbar}{m_\alpha} \mathbf{p}_\alpha(q_k(t)) \cdot \mathbf{d}_\alpha(q_k(t)), \tag{5}$$

and

$$\Omega_k(t) = H_N^{(1)}(q_k(t)) - H_N^{(2)}(q_k(t)). \tag{6}$$

Note, that the kinetic Eqs. (3) and (4) do not utilize any mean-field feature, and the auxiliary functions in (4) evolve on the $S_1$ PES.

The potential energy surfaces in the normal mode approximation and the nonadiabatic coupling vector were obtained by *ab initio* quantum-chemical methods, whereas the initial conditions for the classical trajectories on $S_1$ PES were sampled from the canonical distribution as described in the next section.

### B. Model and simulation procedure

In the present model the harmonic normal mode approximation for the PESs of both the ground and excited states is employed. Although the anharmonicity and the mode couplings play an important role, they can hardly be obtained from the quantum-chemical calculations of polyatomic molecules.

In the harmonic normal mode approximation, the phase space of the PESs can be described in terms of the corresponding equilibrium configuration, the normal modes displacements

$$\boldsymbol{\zeta}^{(\alpha)} = \{\zeta_1^{(\alpha)}, \zeta_2^{(\alpha)}, \ldots\}, \tag{7}$$

where the superscript $\alpha$ labels the PES and their momenta. The transformation matrix between the normal modes displacements and the mass-weighted Cartesian displacements from the equilibrium positions of atomic central is directly available from the Hessian calculation by quantum-chemical software packages.

In the harmonic normal mode approximation the multidimensional trajectory on the PES may be described in terms of the equilibrium configuration, normal modes displacements, and momenta. The former is obtained by the geometry optimization procedure, whereas the frequencies of the normal modes, and the transformation matrix from the mass-weighted cartesian coordinates to the normal modes are directly available from the hessian calculation, both calculations were performed using CASSCF method and the GAMESS U.S. software. The initial conditions for the normal modes oscillators were specified as follows. First, for every normal mode we sample its energy from the canonical distribution by setting[45]

$$E_k = -k_B T \ln \xi, \tag{8}$$

where $\xi$ is the uniform random variate on (0,1). Then, one has the following equations for the time evolution of the mass-weighted displacements

$$\zeta_k(t) = \frac{\sqrt{2E_k}}{\omega_k} \cos(\omega_k t + \varphi_k), \tag{9}$$

and of the corresponding momenta

$$\dot{\zeta}_k = \sqrt{2E_k} \sin(\omega_k t + \varphi_k), \tag{10}$$

where $\omega_k$ and $\varphi_k$ being the frequency and the initial phase of the $k$th normal mode oscillator, respectively. The initial phase for the oscillators was taken random from the interval $(0, 2\pi)$. Thus, at any instant of time we are able to calculate the set of normal modes displacement and momenta for the given trajectory, using Eqs. (9) and (10).

Calculation of the vertical energy splitting between the PESs along the given trajectory requires three quantities, the potential energy for the first PES, counted from its energy minimum, the same quantity for the second PES, and the vertical energy splitting ($\hbar\Omega_0$) between the minima of the PESs. The latter can be obtained from the *ab initio* quantum chemistry calculations and spectroscopic data, see Sec. III C for more details. The vertical energy splitting (in frequency units) can be written as

$$\Omega(t) = \frac{1}{2}\sum_n (\omega_n^{(2)}\zeta_n^{(2)})^2 - \frac{1}{2}\sum_k (\omega_k^{(1)}\zeta_k^{(1)})^2 + \Omega_0, \quad (11)$$

where $\Omega_0$ is counted from the minimum of the second PES, and is positive, if the energy minimum of the second PES lies above the minimum of the first one.

In the following, for the definiteness, we assume that the trajectories evolve on the first PES. The equilibrium geometry, the set of the normal modes, and their frequencies of the second PES are different from those of the first PES, therefore, we have to find how the current molecular configuration is represented by the set of the normal modes displacements on the second PES. This is done in three steps. First, we restore the cartesian coordinates of the molecules from the known set of the normal modes displacements, the transformation matrix between the normal modes and the mass-weighted cartesian displacements, and the equilibrium configuration. Second, we rotate the obtained cartesian configuration to the Eckart frame of the equilibrium configuration of the second PES, since their orientations obtained by the geometry optimization are slightly different. Third, we transform the obtained cartesian coordinates to the normal modes displacements of the second PES, using its equilibrium configuration and the transformation matrix. Then, Eq. (11) is used to obtain the required vertical energy splitting. Note, that the above procedure works for arbitrary Dushinsky rotation in the molecule.

### C. Estimation of the relative energetics of the PESs for *trans*-stilbene and p-coumaric acid

Accurate estimation of the energy splittings between the PESs is of fundamental importance for the modeling and understanding of nonadiabatic reactions. This quantity is also frequently used to examine the quality of quantum-chemical methods, whereas an account for PES-dependent electron correlation energy represents considerable difficulties for the perturbation theories employed there. In particular, the vertical excitation energy for *trans*-stilbene was calculated in Ref. 40 using CASSCF/CASPT2 approach to be 4.07 eV, which is indeed close to the 0–0 transition energy of 4.00 eV.[46] On the other hand, the molecule upon photoexcitation undergoes geometric changes which reduces its energy and may lead to considerably lower 0–0 transition energy than the vertical one.

To estimate the difference between the 0–0 and the vertical transition energies for *trans*-stilbene calculations done in Ref. 40 have been repeated and the vertical excitation energy to the single $^1B_u(HL)$ and double $^1A_g(Z)$ excited states have been obtained using CASPT2 approach. The latter excited state is recognized to play a fundamental role in the process of photoisomerization of *trans*-stilbene, as the radiationless transition into the ground state takes place in the twisted conformation characterized as the double excited one.[16–19] Then the geometries for the excited states of interest have been optimized and the calculations have been repeated. The results are summarized in Table III.

It is well understood that the vertical excitation energies predicted by quantum-chemical calculations are usually not very accurate, but the energy profiles along the given PES are well reproduced. Therefore, we estimate from the data shown in Table III the difference between the 0–0 and the vertical excitation energy for $^1B_u(HL)$ state to be 0.34 eV, which means that the vertical excitation energy is about 4.00+0.34=4.34 eV, where 4.00 eV is the experimentally measured 0–0 transition in the molecular beam.[46–48] The above analysis confirms the intrinsic error of CASPT2 of about 0.3 eV in predicting the vertical excitation energies, and the fact that it usually overestimates the corrections to the CASSCF energies.[49–51]

TABLE III. Vertical excitation energies, corrected by LS (0.3 a.u.)–CASPT2. The energies are in eV and counted from the energy of the ground ($^1A_g(G)$) state at its optimal geometry.

| Electron state | Optimal geometries | | |
|---|---|---|---|
| | $^1A_g(G)$ | $^1B_u(HL)$ | $^1A_g(Z)$ |
| $^1A_g(G)$ | 0.00 | 0.12 | 0.72 |
| $^1B_u(HL)$ | 4.05 | 3.71 | 4.39 |
| $^1A_g(Z)$ | 4.78 | 4.18 | 4.06 |

The $1\ ^1A_g \rightarrow 3\ ^1A_g$ transition was assumed[52] to be responsible for the absorption band with a maximum at 234 nm or 5.3 eV in the two-photon spectrum of *trans*-stilbene dissolved in hexane, which should be close to the vertical excitation energy to $^1A_g(Z)$ state. On the other hand, Table III shows that the difference between the 0–0 and the vertical excitation energies is about 0.72 eV, which yields an estimate of 5.30−0.72=4.58 eV for the 0–0 transition $^1A_g(G) \rightarrow {}^1A_g(Z)$. The results are summarized in the Table IV, where the energies are corrected to be in agreement with the spectroscopical data.

Figure 4 shows the relative energetics of the PESs of *trans*-stilbene, where both the vertical excitation energies and the energies of the PESs minima, counted from the minimum of the ground state PES, are shown. The (local) energy minimum of $S_2$ PES lies above those of $S_1$ state.

Similar approach was employed to estimate the relative energetics of the PESs of p-coumaric acid. The energy difference between the minima of the ground and the $S_1$ PES is taken to be 33 200 $cm^{-1}$ or 4.11 eV (0–0 transition) which is available from the spectroscopical data.[13] The two-photon absorption spectrum is broad with a maximum located at approximately 38 400 $cm^{-1}$ (4.76 eV), and is assumed to be

TABLE IV. The corrected energies of the selected electronic states of *trans*-stilbene. The energy profiles along the given state were taken from the Table I. The relative shifts between the profiles were adjusted to fit the spectroscopical data. For $^1B_u(HL)$ state we used the known value of 4.00 eV for the 0–0 transition, whereas for $^1A_g(Z)$ state we estimated the corresponding vertical excitation energy of 5.30 eV. As in Table I the energies are counted from the energy of the ground state at its optimal geometry.

| Electron state | Optimal geometries | | |
|---|---|---|---|
| | $^1A_g(G)$ | $^1B_u(HL)$ | $^1A_g(Z)$ |
| $^1A_g(G)$ | 0.00 | 0.12 | 0.72 |
| $^1B_u(HL)$ | 4.34 | 4.00 | 4.74 |
| $^1A_g(Z)$ | 5.30 | 4.70 | 4.58 |

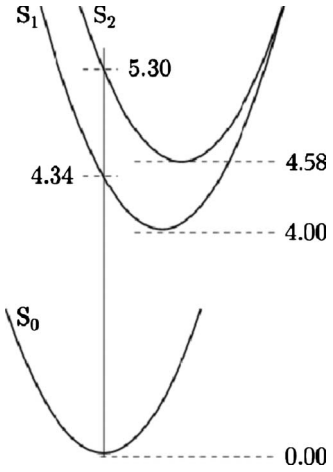


FIG. 4. The relative energies of the PESs of *trans*-stilbene in eV. Both the PESs energy minima and the vertical excitation energies are shown, the data are taken from the Table IV. The PESs are treated as adiabatic (avoided crossings). Here, the nonadiabatic effects arise because the molecule need not to stay on the $S_1$ surface but may undergo transitions to the $S_2$ state. The probability of such a jump increases with decreasing the energy difference between the $S_1$ and $S_2$ curves and with increasing velocity along the reaction coordinate. The X-axis is taken to be the reaction coordinate.

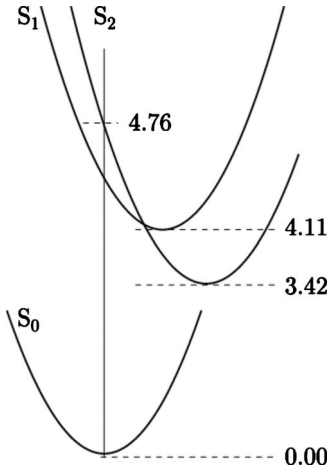


FIG. 5. The relative energies of the PESs of p-coumaric acid in eV. Both the PESs energy minima and the vertical excitation energy $S_0 \rightarrow S_2$ are shown. In the case of p-coumaric acid the PESs are diabatic (allowed crossings). The X-axis is taken to be the reaction coordinate.

the vertical energy splitting between the ground and the $S_2$ PESs, taken at the optimal geometry of the ground state. Thus, in order to obtain the relative energy difference between the $S_2$ and the $S_1$ PESs, we have to estimate the energy difference along the $S_2$ state at the optimal geometry of the ground state and at its optimal geometry. This quantity was found from our *ab initio* calculations on CASSCF(10e/8o) level to be 1.34 eV, and therefore the resulting energy difference between the minima of $S_2$ and $S_1$ states is $-0.69$ eV, which also means that the minimum of $S_2$ state lies below that of $S_1$ state, contrary to the findings for *trans*-stilbene. Note, that we have avoided the direct quantum-chemical calculation of the energy difference between the distinct electronic PESs, which is known to be a considerable problem even for the most sophisticated approaches, only the energy difference along the same PES was used. The obtained results are summarized on Fig. 5.

## IV. PHOTOISOMERIZATION OF POLYATOMIC MOLECULES—RESULTS AND DISCUSSION

### A. Photoisomerization of *trans*-stilbene molecule

For the simulation of the photoisomerization kinetics of *trans*-stilbene we have employed the value of the vertical energy splitting between the minima of the $S_1$ and $S_2$ states of $-0.69$ eV (the minimum of $S_2$ state lies considerably higher than the minimum of $S_1$), which is consistent with the spectroscopical data for both one- and two-photon absorption spectra of *trans*-stilbene. The potential energy surfaces in the normal mode approximation were obtained using the GAMESS U.S. software[53,54] for *ab initio* quantum-chemical calculations and the CASSCF(10e/10o) approach.[49–51] The nonadiabatic coupling vector was calculated with the freely available COLUMBUS (Refs. 55 and 56) quantum chemistry programs suit on the MR-CI level. We mainly concentrate on the investigation of the mechanisms of the photoisomerization rather than on an accurate fitting of the available experimental data. Figure 6 shows the simulated kinetics of the (irreversible) nonadiabatic transition from $S_1$ to $S_2$ state, which is also the photoisomerization kinetics in frames of the considered model assuming nonadiabatic $S_1 \rightarrow S_2$ conversion as the rate limiting step.

The corresponding kinetics is shown in Fig. 6. It has a single-exponential character and is well fitted by the formula

$$\sigma(t) = e^{-t/\tau}, \quad \tau = 630 \text{ ps}. \tag{12}$$

Note, that in our simulation we have neglected the cooling effect of the reaction. Indeed, the molecules with higher total energies, presented in the canonical distribution, should react faster, whereas the molecules with the total energy below some energy threshold may not react at all. Under realistic experimental conditions this leads to the two-exponential decay, with the faster exponent corresponding to the so-called first-order photoisomerization reaction followed by a slower stage when the remaining cold molecules are heated up by the collisions with the bath molecules. Although this cooling

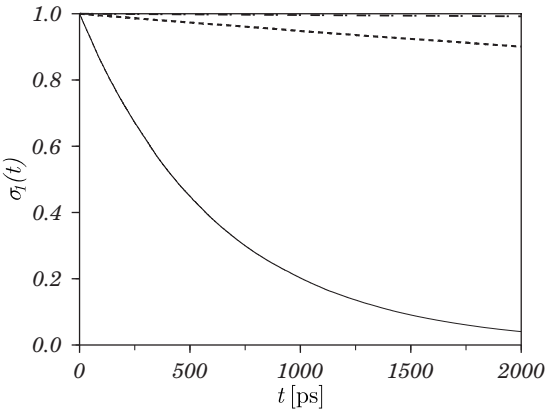


FIG. 6. The kinetics of the nonadiabatic transition from $S_1$ to $S_2$ state for the *trans*-stilbene, solid line. Dashed line shows the kinetic of the nonadiabatic transition from $S_1$ to $S_2$ in the absence of the high-frequency normal modes. Dashed-dotted line shows the kinetic of the nonadiabatic transition from $S_1$ to $S_2$ in the absence of the low and middle frequency normal modes.

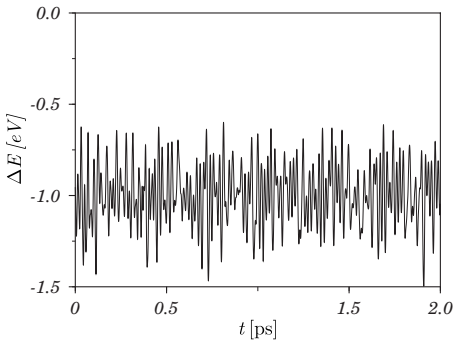


FIG. 7. Time dependence of the vertical energy splitting, for *trans*-stilbene, along a single representative trajectory on $S_1$ PES. It is seen that the surface crossing events are absent (they correspond to the crossing $\Delta E=0$ level).

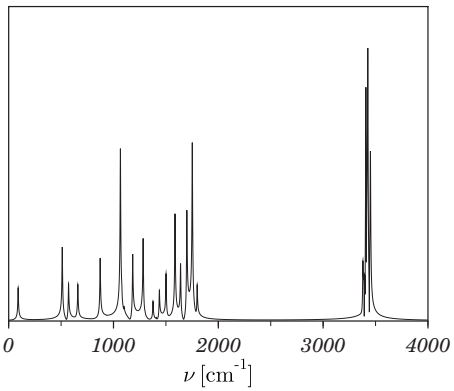


FIG. 8. Absolute value of the Fourier transform of the nonadiabatic couplings V for *trans*-stilbene, averaged over many MD trajectories. Three frequency domains can roughly be defined as the low frequency ($0-500$ cm$^{-1}$), the middle frequency ($500-2000$ cm$^{-1}$), and the high-frequency ($3300-4000$ cm$^{-1}$) domains.

effect can be incorporated into our simulation procedure by assuming the IVR to be faster than the reaction, which is certainly true for the case of *trans*-stilbene, but we analyze in this article the underlying mechanism of the first-order photoisomerization kinetics without influence of the cooling effect.

The obtained results are quite surprising from the standpoint of the standard models of the nonadiabatic transitions, which usually assume the surface crossing events along one or few reaction degrees of freedom. In our simulation the minimum of $S_2$ state lies 0.69 eV *above* the minimum of $S_1$ state, and, therefore, the vertical energy splitting between the PESs at the minimum of $S_1$ state cannot be smaller than 0.69 eV. Thus, the (thermal) energy fluctuations on a single reaction degree of freedom, which may potentially lead to the surface crossing events, have to be about of this value. For stilbene, being in thermal equilibrium at room temperature with its 72 internal degrees of freedom, these are too rare events to contribute to the reaction. Indeed, Fig. 7 shows the vertical energy splitting between the $S_1$ and $S_2$ PESs as the function of time taken along one representative trajectory. The vertical energy splitting fluctuates between $-0.5$ and $-1.5$ eV, but does not exhibit surface crossing events, when the vertical energy splitting passes through the zero mark.

To determine the normal modes being most active in the nonadiabatic coupling between the PESs, we have plotted an absolute value of the Fourier transform of $V_k(t)$ defined in Eq. (5), averaged over many trajectories. This gives us the information about the frequency of the corresponding normal mode and the strength of its contribution into the coupling, see Fig. 8. The distinct frequency domains are clearly seen in Fig. 8. In the low frequency domain with mainly torsional, and bending motion of the molecule, up to $\sim 500$ cm$^{-1}$, one has only one line with a relatively small amplitude. The mid-frequency domain from $\sim 500$ cm$^{-1}$ to $\sim 2000$ cm$^{-1}$, contains a number of lines with different amplitudes. Finally, the high-frequency domain involves normal modes with the dominant contribution of C—H stretch vibrations located around 3300 cm$^{-1}$. The lines in this region are the most intense. In particular this is due to larger velocities of the high-frequency modes, see also Eq. (5).

The dynamics of high-frequency modes is often neglected in *ab initio* simulations of the structural changes of polyatomic molecules, by constraining some bond lengths/angles to their equilibrium values. In the systems with slow reaction modes the above procedure allows to increase the simulation time step considerably, and, as a result, to achieve a longer time scale of the simulation and/or to reduce the computational cost. In order to study the importance of the high-frequency modes for the model under consideration, we have also simulated the dynamics of the nonadiabatic transitions in the absence of the high-frequency vibrations of the stilbene molecule, and have set the initial energy of the corresponding normal mode oscillators to zero when sampling from the thermal distribution. The corresponding kinetics is shown in Fig. 6 by the dashed line. It is readily seen that when removing the high-frequency modes the reaction rate is reduced by a factor of 30, giving the characteristic decay time of about 20 ns. On the other hand, when freezing the low and the middle frequency normal modes and keeping only the high-frequency vibrations of the stilbene molecule, we obtain even a slower reaction with the decay time $>200$ ns.

### B. Photoisomerization of p-coumaric acid molecule

To perform *ab initio* simulations for the case of p-coumaric acid within the framework of the suggested model, first we have to estimate the energy difference between the minima of $S_2$ and $S_1$ PESs. The energy difference between the minima of the ground and the $S_1$ PES is taken to be 33 200 cm$^{-1}$ (0–0 transition), value which is available from the spectroscopical data.[13] The two-photon absorption spectrum found in Ref. 13 is broad and with a maximum located at approximately 38 400 cm$^{-1}$ which is assumed to be the vertical energy splitting between the ground and the $S_2$ PESs, taken at the optimal geometry of the ground state. Thus, in order to obtain the relative energy difference between the $S_2$ and the $S_1$ PESs, we have to estimate the energy difference along the $S_2$ state at the optimal geometry of the ground state and at its optimal geometry. This quantity was found from our *ab initio* calculations on CASSCF(10e/8o) level to be 1.34 eV, and therefore, the resulting energy difference between the minima of $S_2$ and $S_1$ states is $-0.69$ eV, which means that the minimum of $S_2$ state lies below that of

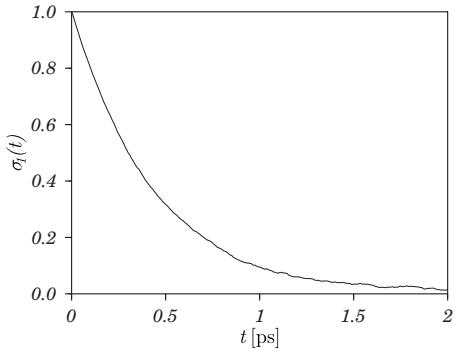


FIG. 9. The kinetics of the nonadiabatic transition from $S_1$ to $S_2$ state for p-coumaric acid. The following set of parameters was used for the simulation: $N=1000$ and $T=270$, where $N$ is the number of MD trajectories and $T$ is the temperature.

$S_1$ state, contrary to the findings for *trans*-stilbene. Note, that we have avoided the direct quantum-chemical calculation of the energy difference between the distinct electronic PESs which is known to be a considerable problem even for the most sophisticated approaches, only the energy difference along the same PES was used.

The simulated kinetics of $S_1 \rightarrow S_2$ transition is shown in Fig. 9, and is indeed very fast compared to the stilbene kinetics, see Eq. (12). The decay has one-exponential character and is well fitted by the formula

$$\sigma(t) = e^{-t/\tau}, \quad \tau = 0.44 \text{ ps}. \tag{13}$$

The reason for the drastic acceleration of the photoisomerization kinetics becomes clear from Fig. 10, where the energy difference between the PESs along some representative trajectory is plotted. Change of the sign of $\Delta E$ indicates the surface crossing event, and there are many of them on the time scale of the reaction. Thus one may conclude that the dominant mechanism of the non-diabatic transitions in p-coumaric acid is via surface crossing events, which explains its much faster isomerization than for stilbene. The high-frequency domain in the nonadiabatic coupling is not

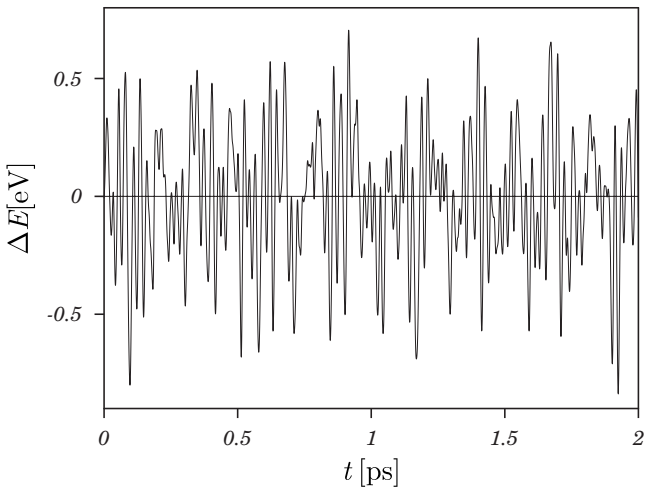


FIG. 10. Time dependence of the vertical energy splitting for p-coumaric acid, along a single representative trajectory on $S_1$ PES and it can be observed that exhibit surface crossing events (they correspond to the crossing of $\Delta E=0$ level).

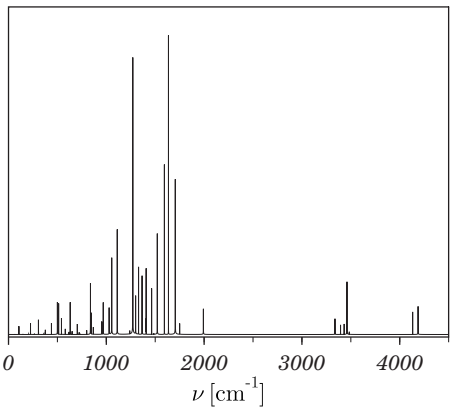


FIG. 11. Absolute value of the Fourier transform of the nonadiabatic couplings V, for p-coumaric acid, averaged over many MD trajectories. Three frequency domains can be roughly defined: the low frequency (0–1000 cm$^{-1}$), the middle frequency (1000–2000 cm$^{-1}$), and the high-frequency (3300–4200 cm$^{-1}$) domains.

well pronounced, see Fig. 11, and removing frequencies higher than 3000 cm$^{-1}$ from the calculations does not considerably affect the kinetics.

## V. CONCLUSION

We have carried out *ab initio* simulations for the *trans-cis* photoisomerization kinetics of two polyatomic molecules, stilbene and p-coumaric acid chromophore. The isomerization after photoexcitation into the first excited state has been modeled as a two-stage process, with the rate limiting step being the nonadiabatic conversion from a single into a double excited state, near the planar geometry of the corresponding *trans*-isomers. The actual isomerization was assumed to take place in the double excited state where it is nearly barrierless and fast. All parameters of the model were estimated either from high-level quantum-chemical methods (equilibrium geometries, normal modes, and their frequencies, nonadiabatic coupling vectors) or from spectroscopical data. The latter were used to obtain the accurate relative energies of the electron states involved in the simulations. The time scale of the photoisomerization kinetics was well reproduced. For gas-phase stilbene at room temperature the nonadiabatic pathway gives a characteristic time of approximately 630 ps, whereas p-coumaric acid photoisomerization under the same conditions is predicted to be faster than 1 ps. A deep insight into the mechanism of the reaction reveals, that in the case of stilbene the nonadiabatic conversion between the single and the double excited states proceeds without surface crossing events, via relaxationlike mechanism, when the intrinsic modes of the molecule play the role of a heat reservoir. On the other hand, the relative energetics of the single and the double excited states in p-coumaric acid is opposite, which leads to frequent surface crossing events on the time scale of the reaction and, as a result, to a much faster photoisomerization.

[1] V. Balzani, *Electron Transfer in Chemistry* (Wiley-VCH, Weinheim, 2001), Vol. I.
[2] R. D. Cannon, *Electron Transfer Reactions* (Butterworths, London, 1980).

[3] L. Eberson, *Electron Transfer Reactions in Organic Chemistry* (Springer-Verlag, Berlin, Heidelberg, 1987).
[4] A. W. Jasper, C. Zhu, S. Nangia, and D. G. Truhlar, Faraday Discuss. **127**, 1 (2004).
[5] J. C. Tully, Faraday Discuss. **110**, 407 (1998).
[6] N. L. Doltsinis, Quantum simulations of complex many-body systems: From theory to algorithm, Lecture Notes **10**, 377 (2000).
[7] M. D. Hack and D. G. Truhlar, J. Phys. Chem. A **104**, 7917 (2000).
[8] A. A. Neufeld, J. Chem. Phys. **121**, 2542 (2004); **119**, 2488 (2003); **119**, 2502 (2003).
[9] D. C. Tranca and A. A. Neufeld, J. Chem. Phys. **130**, 141102 (2009).
[10] J. Troe, Chem. Phys. Lett. **114**, 241 (1985).
[11] D. S. Larsen, Biophys. J. **86**, 2538 (2004).
[12] R. Kort, H. Vonk, X. Xu, W. D. Hoff, W. Crielaarda, and K. J. Hellingwerf, FEBS Lett. **382**, 73 (1996).
[13] W. L. Ryan, D. J. Gordon, and D. H. Levy, J. Am. Chem. Soc. **124**, 6194 (2002).
[14] J. Syage, W. Lambert, P. Felker, A. Zewail, and R. Hochstrasser, Chem. Phys. **88**, 266 (1982).
[15] D. H. Waldeck, Chem. Rev. (Washington, D.C.) **91**, 415 (1991), and references therein.
[16] G. Orlandi and W. Siebrand, Chem. Phys. Lett. **30**, 352 (1975).
[17] G. Orlandi, P. Palmieri, and G. Poggi, J. Am. Chem. Soc. **101**, 3492 (1979).
[18] P. M. Felker and A. H. Zewail, J. Phys. Chem. **89**, 5402 (1985).
[19] F. Negri and G. Orlandi, J. Phys. Chem. **95**, 748 (1991).
[20] J. I. Steinfeld, J. S. Francisco, and W. L. Hase, *Chemical Kinetics and Dynamics*, 2nd ed. (Prentice-Hall, Englewood Cliffs, New Jersey, 1999).
[21] I. W. M. Smith, Chem. Soc. Rev. **37**, 812 (2008).
[22] S. H. Courtney, M. W. Balk, L. A. Philips, S. P. Webb, D. Yang, D. H. Levy, and G. R. Fleming, J. Chem. Phys. **89**, 6697 (1988).
[23] A. Meyer, J. Schroeder, and J. Troe, J. Phys. Chem. A **103**, 10528 (1999).
[24] R. E. Weston, Jr. and J. R. Barker, J. Chem. Phys. A **110**, 7888 (2006).
[25] A. Warshel, J. Chem. Phys. **62**, 214 (1975).
[26] C. J. Finder, M. G. Newton, and N. L. Allinger, Acta Crystallogr., Sect. B: Struct. Crystallogr. Cryst. Chem. **30**, 411 (1974).
[27] J. A. Bouwstra, A. Schouten, and J. Kroon, Acta Crystallogr., Sect. C: Cryst. Struct. Commun. **40**, 428 (1984).
[28] W.-G. Han, T. Lovell, T. Liu, and L. Noodleman, Phys. Chem. Chem. Phys. **3**, 167 (2002).
[29] M. Traetteberg, E. B. Frantsen, F. C. Mijlhoff, and A. Hoekstra, J. Mol. Struct. **26**, 57 (1975).
[30] S. P. Kwasniewski, L. Claes, J.-P. Francois, and M. S. Deleuze, J. Chem. Phys. **118**, 7823 (2003).
[31] L. H. Spangler, R. van Zee, and T. S. Zwier, J. Phys. Chem. **91**, 2782 (1987).
[32] A. A. Heikal, J. S. Baskin, L. Banares, and A. H. Zewail, J. Phys. Chem. A **101**, 572 (1997).
[33] J. S. Baskin, L. Banares, S. Pedersen, and A. H. Zewail, J. Phys. Chem. **100**, 11920 (1996).
[34] S. Nordholm and A. Baeck, Phys. Chem. Chem. Phys. **3**, 2289 (2001).
[35] J. Qian, S. L. Schultz, and J. M. Jean, Chem. Phys. Lett. **233**, 9 (1995).
[36] P. M. Felker, W. R. Lambert, and A. H. Zewail, J. Chem. Phys. **82**, 3003 (1985).
[37] L. Banares, A. A. Heikal, and A. H. Zewail, J. Phys. Chem. **96**, 4127 (1992).
[38] T. Elsaesser and W. Kaiser, Annu. Rev. Phys. Chem. **42**, 83 (1991).
[39] J. W. Perry, N. F. Scherer, and A. H. Zewail, Chem. Phys. Lett. **103**, 1 (1983).
[40] V. Molina, M. Merchan, and B. O. Roos, J. Phys. Chem. A **101**, 3478 (1997).
[41] T. Gensch, C. C. Gradinaru, I. H. M. van Stokkum, J. Hendriks, K. J. Hellingwerf, and R. van Grondelle, Chem. Phys. Lett. **356**, 347 (2002).
[42] N. Mataga, H. Chosrowjan, and S. Taniguchi, J. Photochem. Photobiol., A **5**, 155 (2004).
[43] K. Heyne, O. F. Mohammed, A. Usman, J. Dreyer, E. T. J. Nibbering, and M. A. Cusanovich, J. Am. Chem. Soc. **127**, 18100 (2005).
[44] A. A. Neufeld, J. Chem. Phys. **122**, 164111 (2005).
[45] M. P. Allen and D. J. Tildesley, *Computer Simulation of Liquids* (Oxford University Press, New York, 1987).
[46] B. B. Champagne, J. P. Pfansfiel, D. F. Plusquellic, D. W. Pratt, W. M. van Herpen, and W. L. Meerts, J. Phys. Chem. **94**, 6 (1990).
[47] J. Stangl, V. Holy, and G. Bauer, Rev. Mod. Phys. **76**, 725 (2004).
[48] V. A. Shchukin and D. Bimerg, Rev. Mod. Phys. **71**, 1125 (1999).
[49] K. Andersson, P. Malmqvist, B. O. Roos, A. J. Sadlej, and K. Wolinski, J. Phys. Chem. **94**, 5483 (1990).
[50] S. Yamanaka, M. Okumura, K. Yamaguchi, and K. Hirao, Chem. Phys. Lett. **225**, 213 (1994).
[51] M. Okumura, K. Yamaguchi, and K. Awaga, Chem. Phys. Lett. **228**, 575 (1994).
[52] K. Fuke, S. Sakamoto, M. Ueda, and M. Itoh, Chem. Phys. Lett. **74**, 546 (1980).
[53] M. W. Schmidt, K. K. Baldridge, J. A. Boatz, S. T. Elbert, M. S. Gordon, J. H. Jensen, S. Koseki, N. Matsunaga, K. A. Nguyen, S. Su, T. L. Windus, M. Dupuis, and J. A. Montgomery, J. Comput. Chem. **14**, 1347 (1993).
[54] M. S. Gordon, M. W. Schmidt, C. E. Dykstra, G. Frenking, K. S. Kim, and G. E. Scuseria, *Advances in Electronic Structure Theory: GAMESS a Decade Later* (Elsevier, Amsterdam, 2005).
[55] H. Lischka, M. Dallos, P. G. Szalay, D. R. Yarkony, and R. Shepard, J. Chem. Phys. **120**, 7322 (2004).
[56] M. Dallos, H. Lischka, R. Shepard, D. R. Yarkony, and P. G. Szalay, J. Chem. Phys. **120**, 7330 (2004).